ELSEVIER

Atomically precise self-assembly of one-dimensional structures on silicon

I. Barke, T.K. Rügheimer, Fan Zheng, F.J. Himpsel *

Department of Physics, UW-Madison, 1150 University Avenue, Madison, WI 53706, United States

Abstract

This work has three main themes: (1) fabricate atomically precise nanostructures at surfaces, particularly nanowires consisting of atom chains; (2) explore the behavior of one-dimensional electrons in atomic chains; (3) find the fundamental limits of data storage using an atomic scale memory. Semiconductor surfaces lend themselves towards self-assembly, because the broken covalent bonds create elaborate reconstruction patterns to minimize the surface energy. An example is the large 7×7 unit cell on Si(1 1 1), which can be used as building block. On semiconductors, the surface electrons completely de-couple from the substrate, as long as their energy lies in the band gap. Angle-resolved photoemission reveals surprising features, such as a fractional band filling and a spin-splitting at a non-magnetic surface. An interesting by-product is a memory structure with self-assembled tracks that are five atom rows wide and store a bit by the presence or absence of a single silicon atom. This toy memory is used to test the fundamental limits of data storage and to see how storage on silicon compares to storage in DNA.
© 2007 Elsevier B.V. All rights reserved.

1. Introduction

Nanostructures can be produced by two generic methods, lithography and self-assembly. Lithography becomes more difficult for smaller structures, while self-assembly becomes easier. Below a certain size, it is possible to produce atomically precise structures. This regime will be explored in the following. A particularly interesting aspect is the assembly of atomic chains at surfaces [1]. These come close to the ideal nanowire, an infinite chain of atoms freely suspended in space. Such a wire is nearly impossible to produce experimentally. Free-standing chains of metal atoms can be sustained up to about four atoms in length [2–4], but they are rather unstable. As we will show in the following, it is possible to form rigid atom chains at vicinal Si(1 1 1) surfaces, which combine the best of two worlds: the atoms are firmly locked to the surface (usually in substitutional silicon atom sites). The metallic

electrons, on the other hand, are de-coupled from the silicon substrate. There are no bulk states in the band gap that could hybridize with the surface states. A large variety of such atomic chain structures has been discovered in recent years, which provide a new playground for exploring the physics of electrons as they approach the one-dimensional limit.

One-dimensional physics is particularly simple and elegant. Many problems can be solved analytically. Some problems involving highly correlated electrons can only be solved at all in one dimension. Whole books have been written about this topic [5,6]. One of the peculiar features of electrons in one dimension is the breakdown of the single-electron picture. Theory predicts that the single-electron picture breaks down in a one-dimensional solid. This statement can be rationalized rather simply: electrons cannot avoid each other when moving along the same one-dimensional line. A single excited electron creates a domino effect by colliding with a nearby electron, which collides with the next electron, and so on. This strong interaction has startling consequences on the physics of one-dimensional systems leading to a variety of unusual phases at low temperatures. The most striking prediction is the breakup

* Corresponding author.
 E-mail address: fhimpsel@wisc.edu (F.J. Himpsel).

of electrons into separate spin and charge excitations, the spinons and holons [5]. A variety of other interesting phases exist for one-dimensional systems, such as Peierls-insulators, charge density waves, spin density waves, singlet and triplet superconductivity, and so on [6].

2. Self-assembly of one-dimensional structures

The ever-increasing sophistication in the preparation of single crystal surfaces has made it feasible to tailor surfaces in many ways. The arrival of scanning tunneling microscopy has provided a much more critical look at the perfection of surfaces than diffraction methods, which emphasize the ordered part of the surface. That has helped controlling surfaces more precisely and producing large areas of defect-free surfaces. One-dimensional structures can be prepared by using stepped surfaces as templates. Particularly well suited are surfaces with large unit cells, such as Si(1 1 1)7 $\times$ 7 and Au(1 1 1). The steps become very straight in this case, because the formation of a kink requires adding many extra atom rows, for example 2 $\times$ 7 = 14 rows for Si(1 1 1)7 $\times$ 7. As a result, atomically straight step edges with a length of 20,000 edge atoms have been achieved on Si(1 1 1)7 $\times$ 7 by a simple sequence of anneals [7,8]. This requires of course an accurate azimuthal cut of the Si wafer. The length of kink-free terraces can be extended by heating the wafer with DC current parallel to the steps and keeping it strain-free during heating. A current parallel to the steps causes bunching of the kinks into large facets due to electromigration [9,10].

The step spacing can be controlled by taking advantage of the step–step interaction via their strain field [11]. A repulsive step–step interaction favors equi-spaced steps. The steps need to spaced together closely to provide an interaction large enough for an atomically perfect step spacing. This happens for vicinal Si(1 1 1) at a step spacing of about 6 nm, as shown in Fig. 1 (from [12]). This Si(5 5 7)3 $\times$ 1 surface structure consists of a triple step and a terrace containing a single 7 $\times$ 7 unit cell. The period of this atomic scale grating is known very accurately since the lattice constant of Si is a secondary length standard (compare the number of significant digits given in Fig. 1). Such structures are being studied as possible length standards in the nanoscale regime, which are important for getting an accurate overlay in lithography of microelectronic devices. While lithography becomes more difficult when pushing towards smaller dimensions, self-assembly becomes easier. Bridging the gap between self-assembly and lithography and combining the best of both methods has become an important goal for nanotechnology. Here we are concerned with pushing atomically precise self-assembly to larger dimensions. The 6 nm period in Fig. 1 is typical of the largest structures that can be obtained at surfaces with atomic perfection of wide areas. The building blocks for such structures are typically 50 atoms in size, for example the 7 $\times$ 7 unit cell, the C_{60} fullerene, and the "magic" Au_{55} cluster. It will be interesting to see whether the size of perfectly self-assembled structures can be increased. Another alternative would be a directed assembly process, where a coarse grid is defined by lithography (either
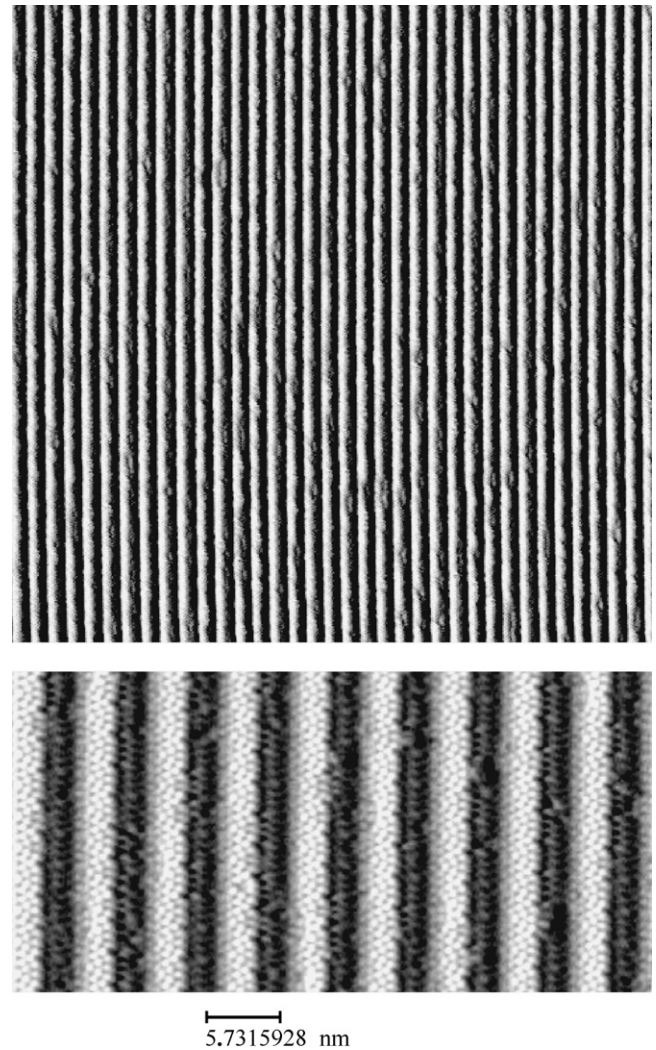

5.7315928 nm

Fig. 1. Step structure created on Si(5 5 7), a vicinal Si(1 1 1) surface. Atomic perfection is achieved by using the large Si(1 1 1)7 $\times$ 7 unit cell as building block (bright stripes) and having the steps close enough to strongly interact with each other. This, and all following STM images show the derivative of the topography in the *x*-direction, which gives the impression of illumination from the left. From [12].

conventional optical lithography or EUV interference lithography [13]) and then filled in by self-assembly.

Stepped surfaces can be converted into atomic chain structures by depositing a sub-monolayer of metal atoms, most notably gold [1]. Typical growth parameters are a substrate temperature of 600–700 °C during Au deposition and a subsequent post-anneal to 800–900 °C for a few seconds with slow cool-down over several minutes. An example is given in Fig. 2a, where the Si(5 5 7) surface from Fig. 1 is converted to a chain structure by 0.2 of a monolayer of Au. This method works for a large group of metal atoms (alkalis, alkaline earths, In, Ag, Au, Pt, and rare earths). These comprise valence states from 1 to 3, s-, p-, d-, and f-electrons, and magnetic atoms. Even the flat Si(1 1 1) surface forms one-dimensional chain structures with three domains. A single domain can be selected by choosing a small miscut of about 1–2°. Apart from the Si(1 1 1) surface, which has the advantage of a large unit cell, there are several
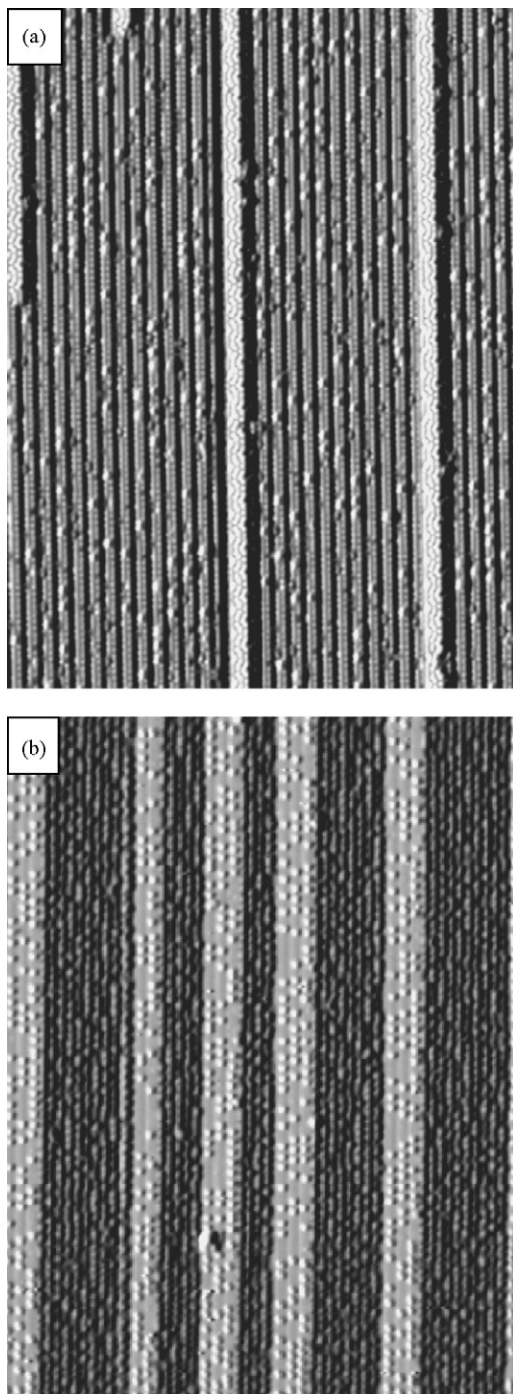
Fig. 2. STM images of Au chain structures on Si(5 5 7) vs. coverage (image width 66 nm): (a) at an under-coverage of 0.02 monolayer below the optimum 0.2 monolayer, most of the surface is converted to a double-chain structure with Si dopant atoms on top of the chains. The remaining part of the surface still exhibits single 7×7 facets of the clean Si(5 5 7) surface (compare Fig. 1). (b) At an over-coverage of 0.2 monolayer, the surface disproportionates into shallower and steeper facets consisting of Si(1 1 1)5×2-Au (bright) and Si(3 3 5)-Au (dark).

other semiconductor surfaces supporting atomic chains, for example Si(1 0 0), SiC(1 0 0), Ge(1 0 0), and GaAs(1 1 0).

Metallic chains are of particular interest. The electrons at the Fermi level are responsible for most of the instabilities towards exotic phases. Such structures may also be considered as the ultimate nanowires, while an insulating wire or a metallic wire on a metallic substrate would not qualify. Not all chain structures are metallic, but we have found that Au chains are metallic for all vicinal Si(1 1 1) surfaces studied so far [1,14]. That includes surfaces tilted towards $[\bar{1}\,\bar{1}\,2]$ with nominally two broken bonds at the step edge, such as (3 3 5), (3 3 7), (5 5 7), as well as surfaces tilted towards $[1\,1\,\bar{2}]$ with one broken bond at the edge, such as (1 1 0), (5 5 3), (7 7 5), (9 9 5), (13 13 7). Even the flat Si(1 1 1) surface breaks its three-fold symmetry and forms the Si(1 1 1)5×2-Au chain structure. It appears that all vicinal Si(1 1 1) surfaces with odd Miller indices form chain structures. By going to shallower tilt angles it is possible to increase the chain spacing and to decrease two-dimensional coupling in a systematic way. Another notable metallic structure is Si(1 1 1)4×1-In [15]. It has a higher coverage than the other chain structures and contains four In chains per unit cell, in contrast to one or two for Au.

Already the growth behavior of the Au chain structures is highly one-dimensional, as shown in Fig. 2a. Here the Au coverage is slightly less than the ideal coverage of 1 chain per unit cell (0.2 monolayer for Si(5 5 7)). As a result, one finds residual patches of clean Si(1 1 1)7×7 that have not been converted yet. These consist of long strips of single 7×7 unit cells, which are in the process of being consumed by Au chains. In fact, an accurate Au coverage is the single most important criterion for preparing high quality chain structures. To pinpoint the coverage dependence of these structures, we have turned to growing "wedges" with a mobile shutter, where the Au coverage varies from 0 to 1 monolayer along the length of the sample ($\approx$10 mm). A large variety of mixed phases can be seen between the stoichiometric structures by STM. Fig. 2b shows one of these phases, where the Si(5 5 7)-Au phase disproportionates into shallower and steeper facets consisting of Si(1 1 1)5×2-Au (bright) and Si(3 3 5)-Au (dark). This occurs at a Au coverage of 0.4 monolayer, well beyond the optimum 0.2 monolayer. Facet formation has been encountered on many other vicinal Si(1 1 1)-Au structures [16]. At even higher coverage (approaching 1 monolayer), the two-dimensional Si(1 1 1)$\sqrt{3} \times \sqrt{3}$ structures tend to take over, which consist of metal trimers. Wedges can be scanned by LEED and photoemission to reveal the changes in the atomic and electronic structure.

With so many chain structures forming on vicinal Si(1 1 1) surfaces, and even on flat Si(1 1 1), it is natural to ask whether there is a common structural feature that stabilizes the chains. In fact, total energy calculations for chain structures induced by alkalis, alkaline earths, and noble metals suggest a common feature, the honeycomb chain [17,18]. A graphitic strip of Si atoms covers a bulk-like Si(1 1 1) surface and forms one of the most stable configurations for the Si(1 1 1) surface. The various metal atoms seem to act as catalysts for forming the honeycomb chain, possibly by bridging the gap between the graphitic part and the rest of the Si(1 1 1) surface. Many different metals can play the same role. The graphitic stripes can be extremely long (hundreds of nanometers), but they are less than two hexagons wide. That suggests nearly perfect lattice match along the stripe (in the $[1\,\bar{1}\,0]$ direction), but a very poor match perpendicular to
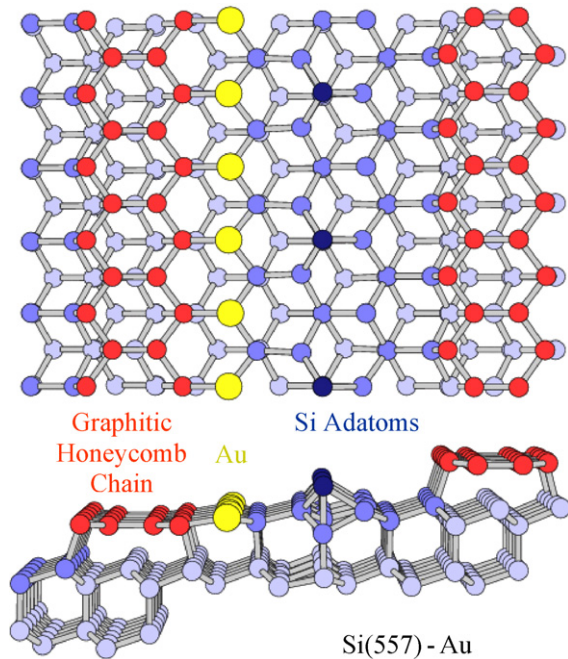
Fig. 3. The structural elements of Au-induced chain structures on vicinal Si(1 1 1) surfaces, demonstrated by a model of the Si(5 5 7)-Au surface obtained from X-ray diffraction [19] and total energy calculations [14,20]. The key element driving these chain structures one-dimensional is the honeycomb chain, a strip of graphitic Si surface atoms (red). The Au chain (yellow) is located at the center of the terrace in substitutional sites, contrary to expectations from step flow growth. (For interpretation of the references to color in this figure legend, the reader is referred to the web version of the article.)

it (in the $[\bar{1}\,\bar{1}\,2]$ direction). Although absent in bulk silicon, π-bonding is quite common at silicon surfaces. It occurs in the π-bonded chain of the Si(1 1 1)2 × 1 cleavage surface and in the π-bonded dimers of Si(1 0 0)2 × 1. Fig. 3 demonstrates the key structural elements of the chain structures, using the Si(5 5 7)-Au structure as example. This model is obtained from a combination of surface X-ray diffraction [19] and total energy calculations [14,20,21].

The Au atom chains are located at the middle of the terrace. They substitute for Si atoms in the outermost layer and become rigidly anchored to three Si atoms underneath. As a result, the position of the Au atoms is barely influenced by the reconstruction at the step edge or by the Si adatoms that double the unit cell along the chains. Naively one would expect the Au atoms to attach themselves to the step edge, where they find high coordination sites. However, these surfaces are full of surprises in their growth behavior and their electronic structure. Apparently, standard principles of epitaxy, such as step flow growth, are not applicable to one-dimensional structures. The finer details of these chain structures have yet to be explored systematically. Despite their fairly small unit cell, there are many possibilities for attaching Si atoms to the step edge. These atoms play an important role in doping the chains to their optimum band filling. This area remains largely unexplored.

A second counter-intuitive feature of chain structures on vicinal Si(1 1 1) is the identity of the atom chains observed by STM. They originate from Si atoms with broken bonds, not from the Au atoms deposited on the surface. The Au atoms pair

their s,p-electron with a neighboring Si bond and create a bound state well below E_F, according to first principles calculations. That is in line with the high electronegativity of Au (higher than Si). The half-filled metallic bands observed by photoemission at these surfaces have mainly Si dangling bond character. Thus, one may view the role of Au more as bystander and catalyst, while the Si bond orbitals form the electronically active wires.

3. The electronic states

The most complete technique for mapping the electronic states at surfaces is angle-resolved photoemission [22,23]. This technique is able to measure the complete set of quantum numbers of surface electrons, most notably their energy E and momentum $\mathbf{p} = \hbar\mathbf{k}$, which consists of the two in-plane components k_x (along the chains) and k_y (perpendicular to the chains). When plotting the photoemission intensity I, the three parameters E, k_x, k_y are typically grouped in two ways, either as band dispersion $I(E, k_x)$ or as Fermi surface $I(k_x, k_y)$. The band dispersion along the chain direction k_x is the most interesting since the perpendicular band dispersion vanishes in the one-dimensional limit. The difference between one- and two-dimensional Fermi surfaces is striking, as shown in Figs. 4 and 5. Two-dimensional Fermi surfaces are characterized by closed curves, such as the Fermi circles observed for the Si(1 1 1)$\sqrt{3} \times \sqrt{3}$-Ag structures doped by additional Ag atoms [24]. A truly one-dimensional Fermi surface consists of two points at $\pm k_F$, but these become straight lines along k_y when plotted in two dimensions. The energy is independent of the momentum k_y perpendicular to the chains (vertical in Figs. 4 and 5).

Chain structures with closely spaced chains, such as Si(5 5 3)3 × 1-Au, display undulating lines. The amplitude of the undulations is a measure of the residual two-dimensional coupling. The complete set of data can be reproduced by a tight binding calculation which uses two couplings along the chains (t_1 and t_3 for first and second neighbor) and one between the chains (t_2). The dimensionality ratio is given by t_1/t_2. For this particular structure one observes a doublet of Fermi lines with $t_1/t_2 = 39, 46$ and a single line with $t_1/t_2 = 12$. For structures with larger chain spacing, such as Si(5 5 7)-Au, the two-dimensional coupling t_2
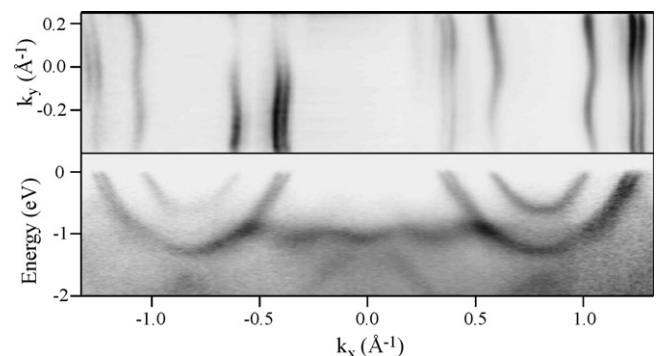

Fig. 4. Fermi surface (top) and band dispersion (bottom) of the Si(5 5 3)-Au chain structure [25]. Two nearly degenerate, half-filled bands are a characteristic of all Au chain structures on vicinal Si(1 1 1) [14]. The splitting has been identified as a spin-splitting induced by the spin–orbit interaction [21,28], quite unexpected for a surface consisting of non-magnetic elements.
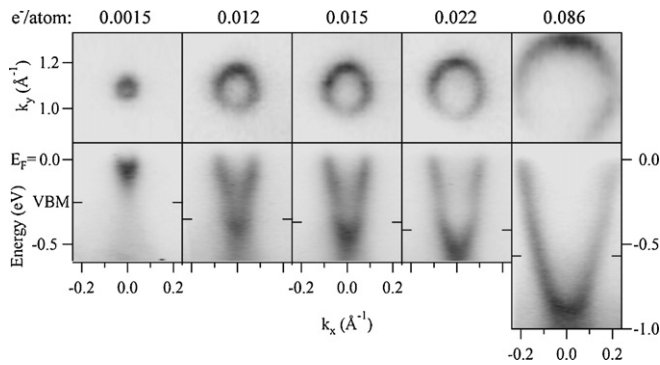
Fig. 5. Fermi surface (top) and band dispersion (bottom) of the two-dimensional Si(1 1 1)$\sqrt{3} \times \sqrt{3}$-Ag structure at various levels of doping with extra Ag atoms (beyond a monolayer). Fermi circles are observed, in contrast to the Fermi lines of one-dimensional structures. The area of the circles increases proportional to the amount of doping. From [24].

becomes too small to be detectable. The angular resolution of the photoemission experiment gives a lower limit of $t_1/t_2 > 70$. This rapid decay of the inter-chain coupling with increasing chain spacing is due to the exponential decay of the wave functions of the dangling bond states that form the half-filled bands. The decay constant is of the order of an atom diameter, while the chain spacing increases from 1.48 to 1.92 nm from Si(5 5 3)-Au to Si(5 5 7)-Au, which is almost two silicon atom diameters.

The observation of two half-filled bands in Fig. 4 [14,25] brings up an intriguing question: why does the surface choose two half-filled bands (corresponding to two broken bonds) instead of one completely filled band (corresponding to a covalent bond). An early explanation in terms of spin-charge separation was put forward in [26]. However, the fact that the splitting does not vanish at E_F [27] rules out such an option (see Fig. 4). Another suggestion for the band splitting invokes the bonding/antibonding interaction between two equivalent broken bonds [27]. Each Au atom is coordinated with three Si atoms underneath, but is only able to form a single bond (for example to the Si atom on the left in Fig. 3). That leaves the two remaining Si atoms with broken bonds (to the right in Fig. 3), which have $p_x + p_y$, $p_x - p_y$ character and thus form a doubly degenerate state. A relativistic local density calculation has been performed for this surface, which describes the observed doublet of half-filled bands quite well [21]. This calculation assigns the bonding/antibonding interaction to a band gap above E_F. The observed band splitting below E_F is assigned to a spin-splitting, which is caused by the spin–orbit interaction in the reduced symmetry at the surface (also known as Rashba effect). Spin–orbit interaction with heavy elements, such as Au, is able to produce spin polarization at the surface of a non-magnetic material. While the net spin polarization integrated over the Brillouin zone remains zero, individual parts of the Brillouin zone become 100% spin-polarized. The resulting one-dimensional spin pattern for the spin-split Fermi surface consists of spins running up and down adjacent Fermi lines. The local density calculation [21] reproduces the two bands seen in photoemission remarkably well. A recent photoemission experiment [28] supports this prediction by resolving the pattern of avoided crossings between the two bands and their back-folded counterparts at the Brillouin

zone boundary (too weak to be seen in Fig. 4). Bands with opposite spin are able to cross each other, while bands with equal spin form an avoided crossing. Other types of splittings in spin-paired, ferromagnetic, and antiferromagnetic bands would give a different pattern, where the two avoided crossings are shifted in E, not in k.

Apart form the intra- and inter-chain coupling there are other important parameters that one would like to vary for getting access to new electronic phases in the one-dimensional phase diagram [5,6]. One of them is the band filling. In two dimensions, the band filling can be varied continuously by adding additional noble metal atoms to the semiconducting $\sqrt{3} \times \sqrt{3}$ monolayer structure of Ag and Au on Si(1 1 1) [24,29]. The photoemission data in Fig. 5 clearly show the expansion of the Fermi circles with an increasing number of electrons provided by additional Ag atoms beyond the one monolayer required for the semiconducting $\sqrt{3} \times \sqrt{3}$ structure. The number of doping-induced electrons per unit cell can be obtained from the area inside the Fermi circle, normalized to the surface Brillouin zone and multiplied by two (for spin up and down). The maximum amount of doping is reached for a $\sqrt{21} \times \sqrt{21}$ superlattice of doping atoms, where the Fermi surface contains about three electrons per $\sqrt{21} \times \sqrt{21}$ unit cell [30]. Compared to bulk doping concentrations, these doping densities are huge. Already the first data point lies beyond the semiconductor-metal transition, as evidenced by the observation of a tiny Fermi circle. This transition is observed in bulk Si at a doping level of 3×10^{21} cm^{-3} [31]. Two-dimensional electrons at surfaces, such as Si(1 1 1)$\sqrt{3} \times \sqrt{3}$-Ag, Au, Si(1 1 1)$\sqrt{7} \times \sqrt{3}$-In [32], or InAs(1 0 0)-Cs [33] could become models for exploring the high density limit of a two-dimensional electron gas.

Doping of one-dimensional chain structures proceeds quite different from the two-dimensional case. Each chain structure automatically selects the optimum density of dopant atoms required for the lowest surface energy [18]. This leads to a well-defined density of Si dopants adsorbed on top of the chains or at the step edge. Typical densities range of 1/40 of a monolayer for Si(1 1 1)5 × 2-Au down to <1/100 of a monolayer for the vicinal surfaces. There is little flexibility in altering the doping by changing the concentration of metal atoms. Nevertheless, different chain structures exhibit different band filling, which allows for discrete variations in the band filling An interesting fractional band filling [25] occurs for the Si(5 5 3)-Au structure shown in Fig. 4 (bottom). The two closely spaced bands are a bit more than half-filled, and the filling of the single band is between one-quarter and one-third. That brings the total filling very close to 8/3 (assuming spin-paired bands) or 5/3 (assuming a spin-split band). Recent calculations [21] and experiments [28] support the spin-polarized scenario. The fractional filling raises questions about a possible analog to the fractional quantum Hall effect in one-dimensional. It is not obvious, though, whether two-dimensional Landau orbits exist in an array of loosely coupled one-dimensional chains. The spectroscopy of one-dimensional chains in a high magnetic field is uncharted territory with great potential, judging from the success achieved with two-dimensional systems.

One-dimensional chain structures exhibit several other interesting features that go beyond the scope of this brief overview, such as nanometer-scale phase separation of a chain into metallic and semiconducting sections [34] (which is related to a conflict between the optimum doping and the periodicity dictated by the Fermi surface [18,35]), Peierls transitions that vary from one band to the other [36,37], and the appearance of a zero-dimensional surface state at the end of a finite chain [38], the existence of a fractional charge at such an end point [39,40], one-dimensional plasmons [41], anisotropic conductivity [42], and a variety of charge density waves [15,36,43] with large fluctuations [44] spreading out the phase transitions.

4. Fundamental limits of data storage

Being able to assemble surface structures with atomic precision makes it possible to fabricate electronic devices with atomic dimensions [45]. These can be used to leapfrog Moore's law of silicon technology by decades and thereby explore the fundamental device limits. Information theory imposes limits on the performance of electronic devices, as shown in Table 1 [46–49]. The quantum conductance determines the maximum conductance through a single string of orbitals in an atomic chain, which corresponds to a single band crossing the Fermi level. The Landauer formula determines the minimum energy to switch one bit at a given temperature. The fastest possible switching time is determined by the energy per bit via the uncertainty relation. And Feynman gave a limit for the propagation of a bit through a wire.

The Si(1 1 1)5 × 2-Au structure lends itself to be used as model for an atomic scale memory [45]. It consists of atomically precise tracks that are 5 Si rows wide (1.67 nm) with extra Si atoms residing on top of the tracks in well-defined 5 × 4 lattice sites (see Fig. 6). Only half of the 5 × 4 sites are occupied, because this corresponds to the optimum density of Si dopants [18]. That suggests using the presence or absence of a Si atom at a 5 × 4 lattice site to store a 1 or a 0. This memory can be written by pre-formatting all 5 × 4 sites with ones and then removing Si atoms with a STM tip where zeros are desired [18,50]. However, mechanical atom manipulation with a STM would take millions of years for writing 1 cm^2, which makes the writing process unsuitable for exploring the limits of electronics.

The interesting part is the readout, which can be done electronically by scanning along a self-assembled track, as shown in Fig. 7. The bits are located at well-defined lattice positions, and each bit has exactly the same signal shape. These features enable sophisticated noise filtering schemes, such as those used in hard disk technology, the densest storage technology on the market. By filtering out all signals different
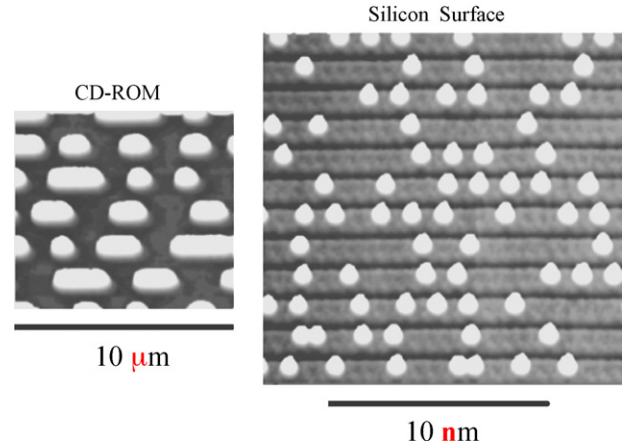

Fig. 6. The Si(1 1 1)5 × 2-Au chain structure, which exhibits extra Si atoms on top of the chains in a half-filled 5 × 4 lattice. This surface has been used to construct an atomic-scale memory, where a bit is stored by the presence or absence of an extra Si atom [45].

from the expected shape, one can eliminate an overwhelming fraction of random noise. In hard disk technology, there is a figure of merit defined for this purpose:

$$\frac{S}{N} = \frac{2}{\pi} \frac{\text{width} \times \text{spacing}}{\text{Jitter}^2} \tag{1}$$

A typical figure of merit is 200/1, which yields a raw error rate of 10^{-8} after noise filtering. In commercial hard disks, the error rate is reduced further by many orders of magnitude using error correction, such as parity check. The same figure of merit can be determined for the signal from the atomic scale Si memory in Fig. 7, where a rms noise level of $\delta z = 5$ pm is achieved with a dwell time of 500 μs. The figure of merit comes out to be about 2000/1, 10 times better than for a hard disk. One should hasten to qualify this result by the observation that the encoding process is very different between the two situations. Hard disks operate with a non-return-to-zero signal, where the
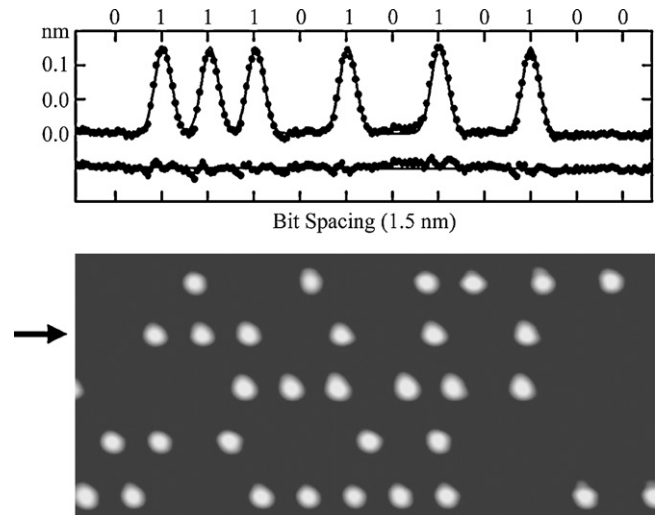

Fig. 7. Readout of the atomic scale memory by a line scan along the chains (500 μs/point). The lower curve demonstrates the reproducibility of the signal by subtracting identical Gaussians located at 5 × 4 lattice sites. That is important for efficient noise filtering. From [45].

Table 1
Limits of electronics from information theory [46–49]

Conductance per channel [46]	$G \le 2e^2/h$
Energy to switch one bit [47]	$E \ge k_BT \ln 2$
Time to switch one bit	$t \ge h/E$ (E is the energy per bit)
Energy to transport a bit [48]	$E \ge k_BT(\nu/c)d$ (d is the distance and ν is the bit rate)

magnetization is either up or down (plus or minus), but zero only during switching. CDs and DVDs use the same kind of signal. The atomic silicon memory, however, has zero as baseline, with a positive pulse for each bit. That resembles the signals propagating in an optical fiber. Nevertheless, a quantitative study of the noise limit is able to extract hard numbers for the limits of the data rate in an atomic scale silicon memory. These can be compared to the actual noise in Fig. 7 and the data rate achieved there. The two main contributions to the noise limit are calculated in Ref. [45], i.e., statistical noise and thermal noise. Their respective spectral densities are $S_s(\omega) = 2eI$ and $S_t(\omega) = 4k_BT/R$ (I is the tunnel current and R is the tunnel junction resistance). The resulting fluctuations in the tunneling current are 8 and 1.3 fA Hz$^{-(1/2)}$ for the conditions of Fig. 7, i.e., $I = 0.2$ nA, $V = 2$ V, $R = 10^{10}\ \Omega$, $T = 300$ K. (The thermal noise is small, because the tunneling electrons have a kinetic energy of 2 eV, which is large compared to $k_BT = 25$ meV.) The actual data in Fig. 7 are 50 times noisier than the limit due to imperfect electronics (mainly a slow feedback circuit).

Putting all these results together in Fig. 8 provides insight into the future of data storage. Density and data rate, the two key parameters, are plotted on a double-logarithmic scale. Hard disks have been improving on both fronts. The split into two branches is due to the different requirements of desktops (optimized for speed) and mobile devices (optimized for density). The data point for the atomic silicon memory is several orders of magnitude higher in density, but even farther down in data rate. It is interesting to observe that Nature's way of storing data in DNA (the green data point) comes out very close to the atomic memory. Connecting the data points from hard disks with the atomic memory and DNA, one arrives at the prediction that the data rate will eventually have to slow down

when the density approaches atomic (or molecular) dimensions (gray area in Fig. 8). Hard disk technology has evolved further since Fig. 8 was first published in Ref. [18], as indicated by the yellow data point. This could be viewed as the first indication of a slowing data rate. The reason for the slowdown is quite simple: As the size of a bit shrinks, the readout signal decreases and a longer integration time is required to detect the bit with the same signal-to-noise ratio.

The ultimate limits for density and data rate can be quantified for the atomic silicon memory. The density limit is determined by the coupling between adjacent bits. For the Si(1 1 1)5 × 2-Au surface, a unit cell consisting of 5 × 4 = 20 atoms is required to separate adjacent bits. The 5 × 4 lattice, in turn, is due to a one-dimensional instability of the Fermi surface at 1/4 filling [35]. Trying to add extra Si atoms onto lattice sites of the underlying 5 × 2 chain structure is only successful 4% of the time due to Si–Si repulsion [51]. For comparison, DNA needs 64 (or 63) atoms to store 2 bits in a base pair, i.e. 32 atoms per bit. The speed limit is given by the statistical noise, which is quantified above. With ideal electronics, and choosing only one data point per bit instead of 10, one could reach the upper end of the gray area in Fig. 8. This is still much lower than the speed of hard disks today, which reiterates the prediction of a slowdown at extreme storage densities. A highly parallel readout will be required to counter this effect.
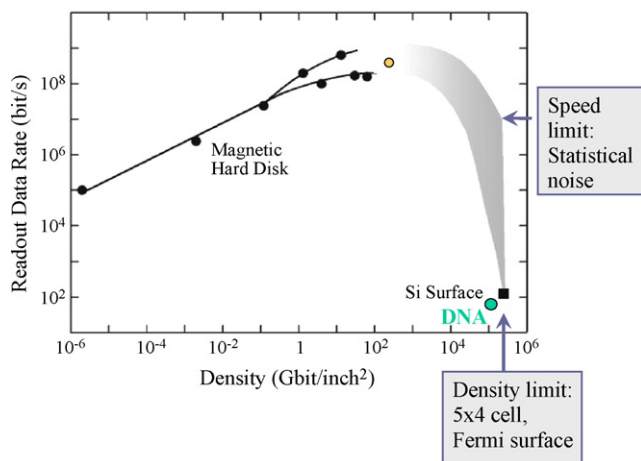
Acknowledgments

Fig. 8. Data rate vs. density for hard disks, compared to the atomic Si memory in Figs. 6 and 7 and to DNA. For densities near the atomic (or molecular) limit, the data rate is reduced dramatically, due to the small readout signal. The density limit is determined by a repulsive interaction between adjacent Si atoms, which limits the unit cell to 5 × 4 = 20 atoms. DNA requires 32 atoms per bit. A new data point for hard disks has been added to the original figure in Ref. [45] (yellow), which seems to provide the first sign of a slow-down in the data rate at high densities. (For interpretation of the references to color in this figure legend, the reader is referred to the web version of the article.)

References

[1] For recent reviews see: J.N. Crain, F.J. Himpsel, Appl. Phys. A, 82 (2006) 431;
    I. Barke, R. Bennewitz, J.N. Crain, S.C. Erwin, A. Kirakosian, J.L. McChesney, F.J. Himpsel, Solid State Commun. 142 (2007) 617.
[2] H. Ohnishi, Y. Kondo, K. Takayanagi, Nature 395 (1998) 780.
[3] V. Rodrigues, D. Ugarte, Phys. Rev. B 63 (2001) 073405.
[4] V. Rodrigues, J. Bettini, P.C. Silva, D. Ugarte, Phys. Rev. Lett. 91 (2003) 096801.
[5] T. Giamarchi, Quantum Physics in One Dimension, Oxford University Press, New York, 2004.
[6] G. Gruner, Density Waves in Solids, Addison-Wesley, Reading, MA, 1994
[7] J. Viernow, J.L. Lin, D.Y. Petrovykh, F.M. Leibsle, F.K. Men, F.J. Himpsel, Appl. Phys. Lett. 72 (1998) 948.
[8] J.L. Lin, D.Y. Petrovykh, J. Viernow, F.K. Men, D.J. Seo, F.J. Himpsel, J. Appl. Phys. 84 (1998) 255.
[9] Y.N. Yang, E.S. Fu, E.D. Williams, Surf. Sci. 356 (1996) 101.
[10] S. Yoshida, T. Sekiguchi, K.M. Itoh, Appl. Phys. Lett. 87 (2005) 031903.
[11] E.D. Williams, R.J. Phaneuf, J. Wei, N.C. Bartelt, T.L. Einstein, Surf. Sci. 294 (1993) 219.
[12] A. Kirakosian, R. Bennewitz, J.N. Crain, T. Fauster, J.L. Lin, D.Y. Petrovykh, F.J. Himpsel, Appl. Phys. Lett. 79 (2001) 1608.

[13] H.H. Solak, C. David, J. Gobrecht, V. Golovkina, F. Cerrina, S.O. Kim, P.F. Nealey, Microelectr. Eng. 67/68 (2003) 56.

[14] J.N. Crain, J.L. McChesney, F. Zheng, M.C. Gallagher, P.C. Snijders, M. Bissen, C. Gundelach, S.C. Erwin, F.J. Himpsel, Phys. Rev. B 69 (2004) 125401.

[15] H.W. Yeom, et al. Phys. Rev. Lett. 82 (1999) 4898.

[16] A.A. Baski, K.M. Saoud, K.M. Jones, Appl. Surf. Sci. 182 (2001) 216.

[17] S.C. Erwin, H.H. Weitering, Phys. Rev. Lett. 81 (1998) 2296.

[18] S.C. Erwin, Phys. Rev. Lett. 91 (2003) 206101.

[19] I.K. Robinson, P.A. Bennett, F.J. Himpsel, Phys. Rev. Lett. 88 (2002) 096104.

[20] D. Sanchez-Portal, R.M. Martin, Surf. Sci. 532 (2003) 655.

[21] D. Sanchez-Portal, S. Riikonen, R.M. Martin, Phys. Rev. Lett. 93 (2004) 146803.

[22] F.J. Himpsel, Adv. Phys. 32 (1983) 1.

[23] S.D. Kevan, Angle-resolved Photoemission, Elsevier, Amsterdam, 1992.

[24] J.N. Crain, M.C. Gallagher, J.L. McChesney, M. Bissen, F.J. Himpsel, Phys. Rev. B 72 (2005) 045312.

[25] J.N. Crain, A. Kirakosian, K.N. Altmann, C. Bromberger, S.C. Erwin, J.L. McChesney, J.L. Lin, F.J. Himpsel, Phys. Rev. Lett. 90 (2003) 176805.

[26] P. Segovia, D. Purdie, M. Hengsberger, Y. Baer, Nature 402 (1999) 504.

[27] R. Losio, K.N. Altmann, A. Kirakosian, J.L. Lin, D.Y. Petrovykh, F.J. Himpsel, Phys. Rev. Lett. 86 (2001) 4632.

[28] I. Barke, F. Zheng, T. Rugheimer, F.J. Himpsel, Phys. Rev. Lett. 97 (2006) 226405.

[29] S. Hasegawa, X. Tong, S. Takeda, N. Sato, T. Nagao, Prog. Surf. Sci. 60 (1999) 89.

[30] J.N. Crain, K.N. Altmann, C. Bromberger, F.J. Himpsel, Phys. Rev. B 66 (2002) 205302.

[31] D.E. Eastman, P. Heimann, F.J. Himpsel, B. Reihl, D.M. Zehner, C.W. White, Phys. Rev. B 24 (1981) 3647.

[32] E. Rotenberg, H. Koh, K. Rossnagel, H.W. Yeom, J. Schafer, B. Krenzer, M.P. Rocha, S.D. Kevan, Phys. Rev. Lett. 91 (2003) 246404.

[33] L.O. Olsson, C.B.M. Andersson, M.C. Hakansson, J. Kanski, L. Ilver, U.O. Karlsson, Phys. Rev. Lett. 76 (1996) 3626.

[34] H.S. Yoon, S.J. Park, J.E. Lee, C.N. Whang, I.W. Lyo, Phys. Rev. Lett. 92 (2004) 096801.

[35] J.L. McChesney, J.N. Crain, V. Perez-Dieste, F. Zheng, M.C. Gallagher, M. Bissen, C. Gundelach, F.J. Himpsel, Phys. Rev. B 70 (2004) 195430.

[36] J.R. Ahn, P.G. Kang, K.D. Ryang, H.W. Yeom, Phys. Rev. Lett. 95 (2005).

[37] J.R. Ahn, J.H. Byun, H. Koh, E. Rotenberg, S.D. Kevan, H.W. Yeom, Phys. Rev. Lett. 93 (2004) 106401.

[38] J.N. Crain, D.T. Pierce, Science 307 (2005) 703.

[39] P.C. Snijders, S. Rogge, H.H. Weitering, Phys. Rev. Lett. 96 (2006) 076801.

[40] W.P. Su, J.R. Schrieffer, Phys. Rev. Lett. 46 (1981) 738.

[41] T. Nagao, S. Yaginuma, T. Inaoka, T. Sakurai, Phys. Rev. Lett. 97 (2006) 116802.

[42] T. Tanikawa, I. Matsuda, T. Kanagawa, S. Hasegawa, Phys. Rev. Lett. 93 (2004) 016801.

[43] J.R. Ahn, H.W. Yeom, H.S. Yoon, I.W. Lyo, Phys. Rev. Lett. 91 (2003) 196403.

[44] G. Lee, J.D. Guo, E.W. Plummer, Phys. Rev. Lett. 95 (2005) 116103.

[45] R. Bennewitz, J.N. Crain, A. Kirakosian, J.L. Lin, J.L. McChesney, D.Y. Petrovykh, F.J. Himpsel, Nanotechnology 13 (2002) 499.

[46] R. Landauer, Z. Phys. B 68 (1987) 217.

[47] R. Landauer, IBM J. Res. Dev. 5 (1961) 183.

[48] R.P. Feynman, Feynman Lectures on Computation, Westview Press, 1996

[49] J. Birnbaum, R.S. Williams, Phys. Today 53 (2000) 38.

[50] G. Dujardin, A. Mayne, O. Robert, F. Rose, C. Joachim, H. Tang, Phys. Rev. Lett. 80 (1998) 3085.

[51] A. Kirakosian, R. Bennewitz, F.J. Himpsel, L.W. Bruch, Phys. Rev. B 67 (2003) 205412.